Nanocrystal Sensors

DOI: 10.1002/ange.201306363

Polyhedral Au–Pd Core–Shell Nanocrystals as Highly Spectrally Responsive and Reusable Hydrogen Sensors in Aqueous Solution**

*Chun-Ya Chiu and Michael H. Huang**

Devices and materials that are capable of selective hydrogen sensing are important for a wide range of applications, including fuel cells, hydrogen-powered vehicles, and hydrogenation reactions. For this reason, materials for hydrogen sensing, such as VO_2 nanowires,[1] cadmium oxide thin films,[2] SnO_2-coated carbon nanotubes,[3] platinum nanowires,[4] and palladium nanowires, films, and disks,[5–8] have been examined extensively. All these H_2 sensors focused on the measurement of hydrogen gas in the air with high sensitivity to low concentrations of hydrogen. However, measurements of electrical or laser-assisted plasmonic signals usually require more complicated sensing-device fabrication and setup. Palladium nanostructures are known to not only interact with hydrogen through surface adsorption, but also incorporate hydrogen and form palladium hydride (PdH).[5–8] Recently, Alivisatos and co-workers demonstrated that the nanogap formed between a triangular Au nanoplate and a Pd nanoparticle can lead to antenna-enhanced spectral shifts upon hydrogen absorption.[9] They subsequently reported the spectral sensing of hydrogen absorption and desorption processes by the use of single Au–Pd core–shell nanocrystals with various shapes.[10] The gold cores should serve as antennae to detect changes in the refractive index of the Pd shells after the diffusion of atomic hydrogen into the shell layer to form PdH. Diffuse spectra on single particles were collected because a mixture of nanocrystal products was synthesized. Triangular plates showed a spectral red shift of approximately 25 nm, but a red shift of less than 4 nm was recorded for icosahedra. Furthermore, unusual blue shifts that were partly attributed to the silicon support were observed for other particle shapes.

We previously synthesized Au–Pd core–shell nanocrystals with various shapes, including tetrahexahedral (THH), cubic, and octahedral structures, by using primarily cubic and octahedral gold cores.[11,12] These nanocrystals are good candidates for the plasmonic sensing of hydrogen because of their size and shape uniformity. The polyhedral gold cores should act as nanoantennae to facilitate the plasmonic-field-enhanced detection of hydrogen absorption and desorption processes. Interestingly, the use of simple nanocrystals in aqueous solution for the direct spectral and possibly visual detection of hydrogen has not been reported before.

In this study, Au–Pd core–shell THH particles, octahedra, and nanocubes were employed as hydrogen-sensing materials. The nanocrystals were dispersed in an aqueous solution in a 10 mL flask, and hydrogen gas was introduced from a balloon into the flask through a syringe (see Figure S1 in the Supporting Information). The presence of dissolved hydrogen was detected. All of these nanocrystals were found to be excellent plasmonic hydrogen sensors: they produced very large red spectral shifts upon hydrogen absorption. THH nanocrystals with exposed high-index facets displayed the largest spectral shifts. All of these particles were highly selective for hydrogen. The spectral shifts were almost fully reversible during successive hydrogen absorption and desorption cycles. For smaller core–shell octahedra, the spectral changes could be observed visually. With all of these advantages, these Au–Pd core–shell nanocrystals should be broadly applicable when simple detection of the presence of hydrogen is desirable.

We prepared Au–Pd core–shell nanocrystals with different morphologies to evaluate their hydrogen-sensing ability (see Figure S2 for the exact reagent amounts used for the synthesis of various Au–Pd core–shell nanocrystals and Figure S3 for their size distribution). Rhombic-dodecahedral, octahedral, and cubic gold nanocrystal cores were synthesized according to our reported methods.[13–15] An aqueous mixture of the surfactant cetyltrimethylammonium chloride (CTAC), polyhedral Au nanocrystals, H_2PdCl_4, and ascorbic acid was made at 31 °C and left for 30 min to enable the formation of the core–shell nanoparticles. In the synthesis of Au–Pd core–shell nanocrystals, we used rhombic-dodecahedral gold cores to demonstrate their use for generating polyhedral core–shell nanostructures (see Figure S4). By simply varying the amount of ascorbic acid used, we could produce Au–Pd tetrahexahedra bound by the {730} facets and octahedra with an average size of approximately 140 nm by using 80 nm rhombic-dodecahedral gold cores (Figure 1 a,b).

Au and Pd have a lattice mismatch of 4.61 %, so the THH morphology may be a manifestation of the release of lattice strain. The Au–Pd octahedra are not geometrically perfect, but show stacking faults and cracks in their appearance as a means to release the lattice strain. Similar morphological features have been observed for Au–Pd octahedra with cubic gold cores.[11] Because of their high size uniformity, the octahedra readily form a monolayer packing structure (Figure 1 b). Since it was difficult to form Au–Pd nanocubes with the rhombic-dodecahedral gold cores, we used 80 nm gold nanocubes and obtained Au–Pd nanocubes with an average size of approximately 110 nm. These nanocubes were not all

[*] C.-Y. Chiu, Prof. M. H. Huang
Department of Chemistry, National Tsing Hua University
Hsinchu 30013 (Taiwan)
E-mail: hyhuang@mx.nthu.edu.tw

[**] This research was supported by the National Science Council of Taiwan (NSC 101-2113M-007-018-MY3).

Supporting information for this article is available on the WWW under http://dx.doi.org/10.1002/anie.201306363.

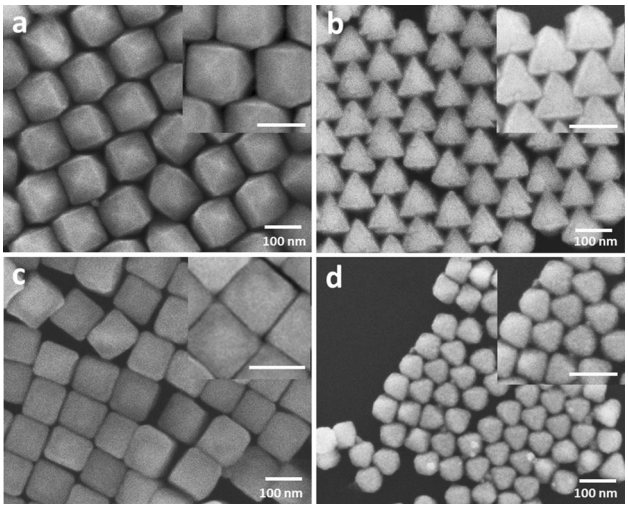

Figure 1. SEM images of the synthesized Au–Pd core–shell a) THH particles, b) octahedra, and c) cubes. d) SEM image of smaller Au–Pd core–shell octahedra formed by the use of octahedral Au cores. Insets show enlarged SEM images. All scale bars show a distance of 100 nm.

perfectly cubic (Figure 1 c). To form Au–Pd octahedra with thinner shells, we used 80 nm octahedral gold cores and obtained particles with an average size of approximately 90 nm (Figure 1 d). These octahedra did not show lattice-strain-induced features, possibly because of the thinner Pd shells. We also synthesized novel Pd–Au core–shell concave cubes with cubic palladium cores to test their ability to sense hydrogen. These particles had a crossed depression in the central region of each cubic face, and the particle shape resembled that of an octopod, with faceted branches at the corners of the cube (see Figure S5). Scanning electron microscopy (SEM) images of the various gold cores and the cubic Pd cores are shown in Figure S4 of the Supporting Information.

To confirm the core–shell particle composition, we characterized these nanocrystals by transmission electron microscopy (TEM). Figure 2 shows TEM images viewed along certain directions, the corresponding selected-area electron diffraction (SAED) patterns, and schematic drawings of the core–shell nanocrystals. Owing to the relatively thick shells, the gold cores cannot be seen easily, except in the case of the Au–Pd octahedron and cube with thinner shells. The SAED patterns match those of palladium. Previous studies have established the exact lattice-orientation relationship between the Au cores and the Pd shells: the (200) and (220) lattice planes of Au are parallel to the respective planes of Pd.[11,12,16] The schematic drawings depict the exact core orientations in these particles. These orientations could be verified on the basis of the high-angle annular dark-field scanning transmission electron microscopy (HAADF-STEM) images of the Au–Pd nanocrystals (see Figure S6 for HAADF-STEM images of the Au–Pd concave cubes; the corresponding STEM-EDS (energy dispersive X-ray spectroscopy) mapping images of the Au and Pd signals are also provided). The HAADF-STEM images showed clearly the rhombic-dodecahedral and cubic cores with core and shell orientations consistent with those shown in Figure 2. EDS elemental mapping images confirmed the presence of polyhedral Au cores and the Pd shells. In the case of the Pd–Au concave cubes, the presence of cubic Pd cores was confirmed.

Figure 3 presents UV/Vis absorption spectra of the Au–Pd core–shell THH particles, octahedra, nanocubes, and smaller octahedra before and after hydrogen absorption. We synthesized octahedra and THH particles with two different average sizes to evaluate the effect of shell thickness on the extent of spectral shifts (Figure 3 a–d). The respective band positions in the UV/Vis spectra of the rhombic-dodecahedral, cubic, and octahedral gold cores were at 558, 565, and 571 nm (see Figure S7 in the Supporting Information). Pd nanocubes with sizes of 22–76 nm have been reported to show an absorption band in the range of 280–470 nm, whereas 110 nm Pd cubes absorb at 580 nm.[17] Pd octahedra with sizes of about 125 nm show an absorption band at 450 nm.[18] On the basis of the known general absorption-band positions of polyhedral Pd nanocrystals, the band at 390–410 nm was attributed to the absorption characteristic of Pd, whereas the position of the more pronounced band depended on the particle size or Pd shell thickness.[11] The emergence of this band (for comparison, see Figure S10 a) and the fact that this band is strongly red-shifted relative to that observed for pristine Pd nanocrystals of similar sizes suggest that the gold cores exert a significant influence on the absorption profile of these core–shell particles. The band is strongly linked to the localized surface plasmon resonance (LSPR) of the gold cores; its position is modulated by the thickness of the Pd shell and the

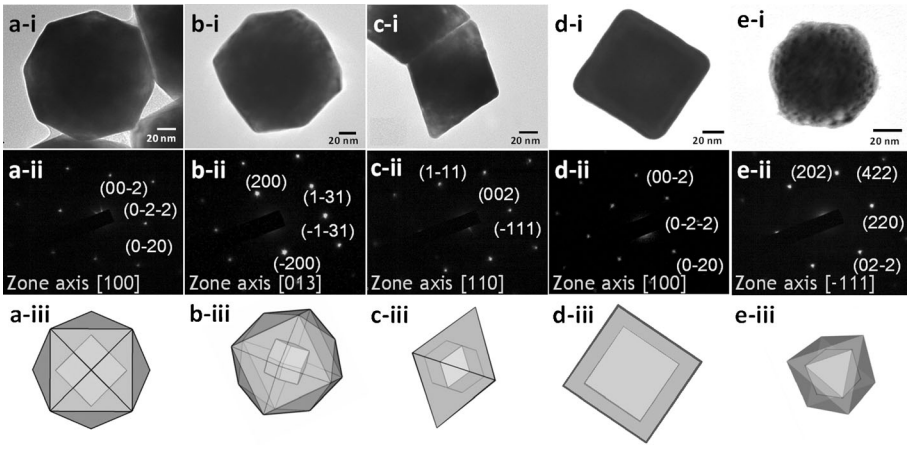

Figure 2. i) TEM images (scale bars: 20 nm), ii) the corresponding SAED patterns, and iii) schematic drawings of the Au–Pd core–shell nanocrystals: a) a tetrahexahedron viewed along the [100] direction; b) a THH nanocrystal oriented along the [310] direction; c) an octahedron viewed along the [110] direction; d) a cube viewed along the [100] direction; e) a smaller octahedron viewed along the [111] direction.

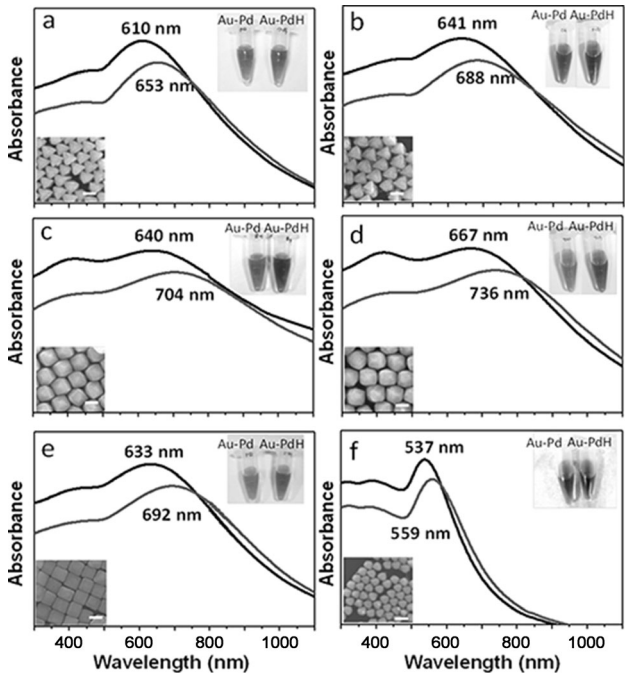

Figure 3. UV/Vis absorption spectra of Au–Pd core–shell nanocrystals: a) 130 nm octahedra; b) 148 nm octahedra; c) 140 nm tetrahexahedra; d) 150 nm tetrahexahedra; e) 110 nm cubes; f) 90 nm octahedra with 80 nm octahedral gold cores. SEM images of the nanocrystals are also shown. The spectra were recorded before (black) and after (gray) the hydrogen-absorption experiment. Photographs of the solutions before (left) and after (right) the hydrogen-absorption experiment are also shown.

overall particle size. Au–Pd core–shell nanobars and nanospheres with thin Pd shells also show predominantly an SPR band due to the Au cores.[19,20]

When the Au–Pd particles were exposed to hydrogen gas dissolved in the solution, the immediate formation of PdH caused a change in the refractive index of the Pd shell, and the absorption spectrum of the particles reported this change.[10] The 140 and 150 nm tetrahexahedra showed the largest red shifts of 64 and 69 nm, respectively. Red shifts of 43 and 47 nm were observed for the absorption bands of the 130 and 148 nm octahedra, respectively. The cubes exhibited a red shift of 59 nm to 692 nm. All of these band shifts are quite significant and indicate that these Au–Pd core–shell nanocrystals are all excellent hydrogen-sensing materials. Particles with larger sizes or thicker Pd shells can further extend the spectral shift. They are the ideal particles to use if very large spectral shifts are desirable.

These results show that various different Pd surfaces are effective for hydrogen adsorption and absorption; it cannot be readily concluded that high-index {730} facets are necessarily more sensitive facets. This view makes sense because hydrogen absorption is conceived to take place largely in the interior of Pd particles. Interestingly, the activation energy barrier for the surface-to-first-subsurface diffusion of hydrogen has been shown to be almost identical for Pd {100} and Pd {111} facets, although a difference in the activation energy exists for hydrogen diffusion from the first to the second subsurface layer.[21,22] The substantial decrease in absorbance and the associated increase in the bandwidth after hydrogen absorption must be related to a compositional change in the Pd shell. The nanocrystal solutions appeared darker after hydrogen absorption. We found that smaller and thinner Au–Pd core–shell octahedra could produce a visual color change for the straightforward detection of hydrogen absorption (Figure 3 f). Although the extent of the band shift (22 nm) is not quite as large as that observed for other Au–Pd nanocrystals examined, the narrower band profile enables the spectral shift to be visually detectable. The solution color changed from purplish red to purple upon hydrogen absorption. Both the band position and the solution color indicate that the band at 537 nm arises from the SPR absorption of the Au cores. We noticed that the response time to hydrogen absorption is very fast for all particles (about 20 s). However, particles with thick Pd shells can take around 1 min to complete the spectral shift.

To further demonstrate the effect of the thickness of the Pd shell on the shift of the Au SPR band upon hydrogen absorption, we used smaller 74 nm octahedral gold cores to synthesize a series of Au–Pd core–shell octahedra with sizes of 75, 80, 87, and 90 nm (see Figure S8). Because the gold core and the Pd shell have the same shape, particles with the uniformly thinnest Pd shells could be obtained (i.e., Pd-shell thicknesses of 0.5 and 3 nm for the 75 and 80 nm octahedra). The Au–Pd octahedra exhibited a pronounced Au SPR band that was markedly blue-shifted from 561 to 515 nm as the thickness of the Pd shell increased. The blue shift occurs because the nanocrystals with thinner Pd shells possess more optical characteristics of Au. After hydrogen absorption, the 87 and 90 nm octahedra with Pd-shell thicknesses of 6.5 and 8 nm displayed spectral red shifts of 26 and 36 nm, respectively; however, the 75 and 80 nm Au–Pd octahedra exhibited red shifts of only 2 and 8 nm, respectively. Thus, only Au–Pd particles with a sufficiently thick Pd shell (5 nm or more) can serve as suitable hydrogen sensors. Our results show that Au–Pd particles with thicker Pd shells and hence a more blue-shifted initial LSPR position owing to greater plasmonic influence by Pd exhibit higher sensitivity to hydrogen.

We also measured the Au SPR band shifts for Au–Pd core–shell THH particles and octahedra with different sizes dispersed in several solvents to investigate the refractive-index sensitivity of the particles (see Figure S9). For all particles, approximately linear red shifts of the absorption band were observed as the refractive index of the solvent increased. However, particles with thick Pd shells (34–38 nm) displayed much higher refractive-index sensitivity than particles with thin Pd shells (3–7 nm). The refractive-index sensitivity was determined to be 442, 399, 167, and 194 nm per refractive index unit (RIU) for 150 nm THH particles (at a Au LSPR position of 667 nm), 148 nm octahedra (at 641 nm), 98 nm octahedra (at 563 nm), and 105 nm octahedra (at 537 nm), respectively. Miller and Lazarides showed through their theoretical study that the refractive-index sensitivity of nanoparticles varies linearly with the plasmonic-resonance wavelength, and that the more red-shifted the LSPR band position of a nanoparticle is, the higher its refractive-index sensitivity is.[23,24] In the case of the Au–Pd bimetallic core–shell system, particles with a more red shifted

initial LSPR position also exhibited generally higher refractive-index sensitivity. However, the thickness of the Pd shell is more important than the starting LSPR position for hydrogen-sensing applications.

It is known that hydrogen diffusion into Pd nanoparticles can cause lattice expansion of the particles. XRD patterns and electron microscopy, particularly SAED patterns, have previously been used to confirm the lattice-constant changes after the diffusion of hydrogen atoms into the palladium lattice.[25,26] To examine whether or not the expansion of the Pd lattice as a result of hydrogen absorption was detectable, we recorded XRD patterns of the 90 nm Au–Pd octahedra with 80 nm gold cores before and after hydrogen absorption (Figure 4). Remarkably, a slight shift in the position of the Pd (111) peak was observed from $2\theta = 40.12$ to 40.02° after

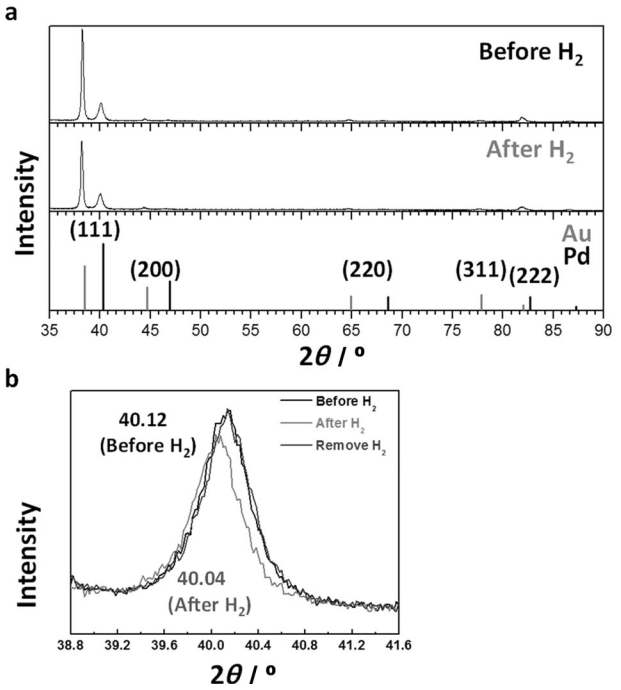

Figure 4. a) XRD patterns of the 90 nm Au–Pd core–shell octahedra with 80 nm octahedral gold cores before and after hydrogen absorption. b) Expanded Pd (111) peak region showing the slight shift in the peak position after hydrogen absorption. The Pd (111) peak returns to its initial position after hydrogen desorption.

hydrogen absorption. This shift in the peak position indicated the occurrence of a slight lattice expansion of the (111) planes from 2.487 to 2.492 Å (or a unit-cell lattice expansion of 0.008 Å) following the incorporation of hydrogen atoms into the lattice even without the application of an external pressure. The Pd (111) peak returned to its initial position when the vial containing the Au–Pd nanocrystals was shaken vigorously and then opened to release hydrogen.

Control experiments were conducted with Pd nanocubes, Pd–Au concave cubes, and Au rhombic dodecahedra as hydrogen-sensing materials (see Figure S10). Pd nanocubes showed a slight band shift from 326 to 332 nm upon exposure to dissolved hydrogen. The spectral profile of the Pd nanocubes after hydrogen absorption to form PdH also displayed decreased absorbance and a significantly broadened bandwidth; thus, the detection of absorbance changes in the range of 550–700 nm can also be used for hydrogen sensing. The Pd–Au concave nanocubes and Au rhombic dodecahedra showed no spectral changes after exposure to hydrogen; they are therefore not useful for hydrogen sensing. The Au–Pd THH particles and octahedra were also exposed to the oxygen gas and carbon monoxide gas for up to 9 min (see Figure S11). No spectral changes were observed after the exposure of the particles to CO, whereas hard-to-detect red shifts of 5 nm or less were recorded for oxygen. The results demonstrate the high selectivity of the Au–Pd nanocrystals for hydrogen.

The various Au–Pd core–shell nanocrystals were evaluated for spectral reversibility in hydrogen absorption and desorption cycles. The absorbed hydrogen could be removed from the nanocrystals simply by vigorously shaking the vial for about 1 min and then taking off the vial cap. The nanocrystals were then ready for the next cycle of hydrogen incorporation and removal. Nearly reversible spectral responses were observed for the Au–Pd THH, octahedral, and cubic nanocrystals, with the absorption band returning to within 10 nm of its original band position (Figure 5). The slight change in the band position is caused by residual

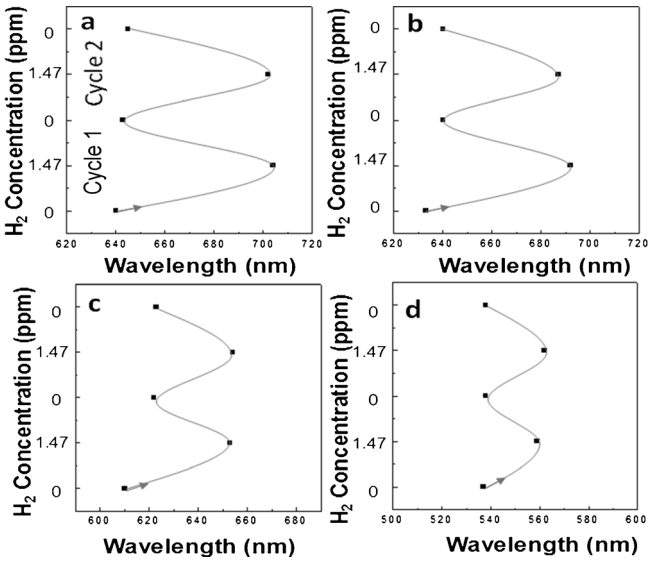

Figure 5. Examination of the spectral reversibility of the various Au–Pd core–shell nanocrystals during hydrogen absorption and desorption cycles. Two cycles of spectral responses are shown for a) 140 nm THH nanocrystals, b) 110 nm nanocubes, c) 130 nm octahedra, and d) 90 nm octahedra.

hydrogen, which is not easy to remove completely. However, a return to the exact first-cycle position was observed in the second cycle. A hydrogen concentration of 1.47 ppm was labeled to indicate the normal concentration of dissolved hydrogen in water at a pressure of 1 atm. With the 90 nm Au–Pd octahedra, nearly full reversibility was observed even in the first cycle. After hydrogen desorption, the solution color looked identical to that of the original solution before exposure to hydrogen (see Figure S12). When this sample

was subjected to ten cycles of hydrogen absorption and desorption, no structural changes were detected; this experiment proved that the nanocrystals really are reusable (see Figure S12). Thus, these nanocrystals can serve as simple and reusable hydrogen sensors based on direct visual observation and should find application in a broad range of situations.

In conclusion, Au–Pd core–shell tetrahexahedral, octahedral, and cubic nanocrystals have been synthesized by the use of polyhedral gold nanocrystal cores by epitaxial overgrowth of a Pd shell in aqueous solution. The core–shell nanocrystals show a pronounced band associated with the surface plasmon resonance absorption of the gold cores for better spectral sensing of hydrogen. The gold cores serve as effective plasmonic antennae and enable the detection of hydrogen at low concentrations on the basis of the very large spectral red shifts observed for the Au–Pd nanocrystals upon exposure to dissolved hydrogen in water. The use of smaller Au–Pd octahedra with thinner Pd shells resulted in a visually detectable change in the color of the solution within 1 min upon hydrogen absorption. No spectral changes were recorded when the particles were exposed to oxygen or CO. The nanocrystals showed nearly reversible spectral shifts during hydrogen absorption and desorption cycles and are therefore promising simple and reusable hydrogen sensors for various applications.

Received: July 22, 2013
Revised: August 28, 2013
Published online: October 7, 2013

Keywords: core–shell nanocrystals · gold · hydrogen sensing · palladium · surface plasmon resonance

[1] E. Strelcov, Y. Lilach, A. Kolmakov, *Nano Lett.* **2009**, *9*, 2322.
[2] P. Dhivya, A. K. Prasad, M. Sridharan, *Int. J. Hydrogen Energy* **2012**, *37*, 18575.
[3] M. Yang, D.-H. Kim, W.-S. Kim, T. J. Kang, B. Y. Lee, S. Hong, Y. H. Kim, S.-H. Hong, *Nanotechnolgy* **2010**, *21*, 215501.
[4] F. Yang, K. C. Donavan, S.-C. Kung, R. M. Penner, *Nano Lett.* **2012**, *12*, 2924.
[5] F. Favier, E. C. Walter, M. P. Zach, T. Benter, R. M. Penner, *Science* **2001**, *293*, 2227.
[6] X. Q. Zeng, M. L. Latimer, Z. L. Xiao, S. Panuganti, U. Welp, W. K. Kwok, T. Xu, *Nano Lett.* **2011**, *11*, 262.
[7] A. Tittl, P. Mai, R. Taubert, D. Dregely, N. Liu, H. Giessen, *Nano Lett.* **2011**, *11*, 4366.
[8] C. Langhammer, I. Zorić, B. Kasemo, *Nano Lett.* **2007**, *7*, 3122.
[9] N. Liu, M. L. Tang, M. Hentschel, H. Giessen, A. P. Alivisatos, *Nature Mater.* **2011**, *10*, 631.
[10] M. L. Tang, N. Liu, J. A. Dionne, A. P. Alivisatos, *J. Am. Chem. Soc.* **2011**, *133*, 13220.
[11] C.-L. Lu, K. Prasad, H.-L. Wu, J.-a. A. Ho, M. H. Huang, *J. Am. Chem. Soc.* **2010**, *132*, 14546.
[12] C.-W. Yang, K. Chanda, P.-H. Lin, Y.-N. Wang, C.-W. Liao, M. H. Huang, *J. Am. Chem. Soc.* **2011**, *133*, 19993.
[13] H.-L. Wu, C.-H. Kuo, M. H. Huang, *Langmuir* **2010**, *26*, 12307.
[14] P.-J. Chung, L.-M. Lyu, M. H. Huang, *Chem. Eur. J.* **2011**, *17*, 9746.
[15] C.-C. Chang, H.-L. Wu, C.-H. Kuo, M. H. Huang, *Chem. Mater.* **2008**, *20*, 7570.
[16] F.-R. Fan, D.-Y. Liu, Y.-F. Wu, S. Duan, Z.-X. Xie, Z.-Y. Jiang, Z.-Q. Tian, *J. Am. Chem. Soc.* **2008**, *130*, 6949.
[17] W. Niu, Z.-Y. Li, L. Shi, X. Liu, H. Li, S. Han, J. Chen, G. Xu, *Cryst. Growth Des.* **2008**, *8*, 4440.
[18] W. Niu, L. Zhang, G. Xu, *ACS Nano* **2010**, *4*, 1987.
[19] K. Zhang, Y. Xiang, X. Wu, L. Feng, W. He, J. Liu, W. Zhou, S. Xie, *Langmuir* **2009**, *25*, 1162.
[20] J.-W. Hu, J.-F. Li, B. Ren, D.-Y. Wu, S.-G. Sun, Z.-Q. Tian, *J. Phys. Chem. C* **2007**, *111*, 1105.
[21] P. Ferrin, S. Kandoi, A. U. Nilekar, M. Mavrikakis, *Surf. Sci.* **2012**, *606*, 679.
[22] D. Shuai, D. C. McCalman, J. K. Choe, J. R. Shapley, W. F. Schneider, C. J. Werth, *ACS Catal.* **2013**, *3*, 453.
[23] M. M. Miller, A. A. Lazarides, *J. Phys. Chem. B* **2005**, *109*, 21556.
[24] K. M. Mayer, J. H. Hafner, *Chem. Rev.* **2011**, *111*, 3828.
[25] D. Jose, B. R. Jagirdar, *Int. J. Hydrogen Energy* **2010**, *35*, 6804.
[26] H. Kobayashi, M. Yamauchi, H. Kitagawa, Y. Kubota, K. Kato, M. Takata, *J. Am. Chem. Soc.* **2008**, *130*, 1828.

